The back reflected radiation is not allowed to hit any detector parts. Only after one more reflection, radiation is scattered into the detector. Here one gets a factor of 1.5 for the ratio of reflection coefficients, due to the difference of the mean reflected energy. These absorbers must be covered by an antireflection coating of 130μm Cu and 500μm Ag on W.

There are still two more differences: 1) In the present arrangement the collimators C1, C2 and C3 absorb about 50% of the power, decreasing the amount of power listed in table 23. On the other hand these absorbers are scattering additional background into the experiment. Assuming that these two influences approximately cancel, one gets a factor of 1 with an upper bound of 2.

The overall ratio of radiation backgrounds is therefore $6.3 \cdot 1 \cdot 1.5 \cdot 1 = 10$; i.e. we have to expect a level of radiation about 10 times larger than at present, normalized to the same electron beam current.

What are the consequences for the ZEUS detector?
The direct reflected synchrotron radiation delivers a dose rate of about 0.01 Gy/s, adding up to about 10^4 to 10^5 Gy/y. The vertex detector, which must of course be shielded from this radiation, receives a dose which is about 1000 times smaller.

The background in the CTD under present running conditions is small and hard to measure. One finds for the average number of background hits per event, which are more or less uniformly distributed through out the drift chamber:

$$N_{hit} = 1.75 + (0.037 \pm 0.016)\frac{I}{\mathrm{mA}}$$

With an electron current of I=58 mA, and a factor of 10, one expects 25$\pm$10 hits, which appears tolerable.

8 Magnet Design

8.1 The Rev1 Magnet Configuration

A schematic representation of the Rev.1 magnet configuration to the left of the IP is shown on Fig. 45 and for the right on Fig. 46 for the ZEUS and H1 experiments. For the Rev.1 lattice the two experiments differ on the left by having an air–core combined function magnet, QH1, for H1 and an iron dominated combined function magnet, QH, for ZEUS. This difference is necessitated both by the more restricted space in H1 at this magnet location and the presence of a large longitudinal magnetic field, which would immediately saturate an iron–dominated magnet. On the right side of both experiments an existing solenoidal compensator magnet is removed and this yields sufficient space on the right for the iron dominated combined function magnet, QH. Thus the ZEUS magnet configuration is left–right symmetric with QH on both sides. The configuration for H1, while functionally symmetric, does differ in having QH1 on the left and QH on the right.

The electron and proton beams are separated into separate beam pipes at $\pm$11 m in the magnetic septum quadrupole QM. The inner combined function magnets QG and QH provide some central focusing for the electrons as well as the 8 mrad separation angle between the beam lines. The QI and QJ quadrupoles complete the inner focusing for the electrons and are

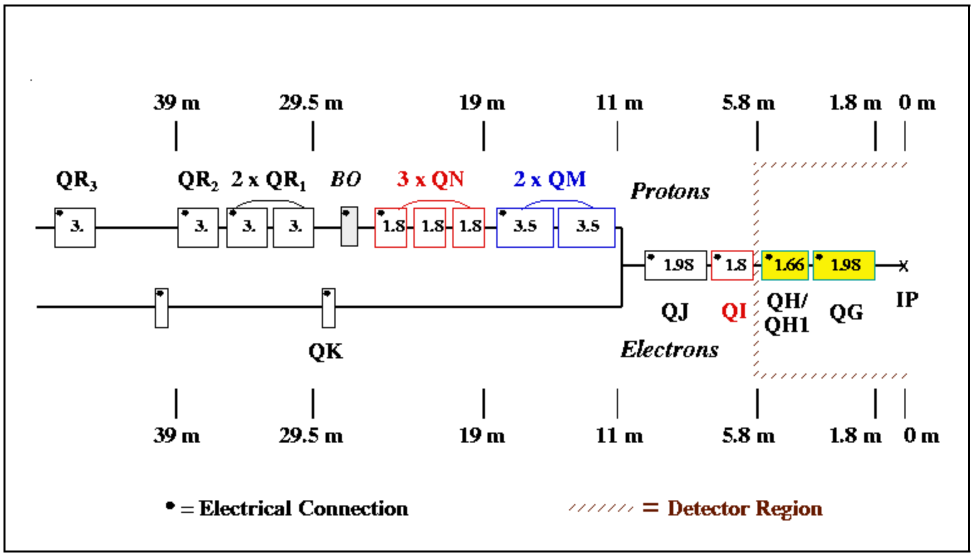

Figure 45: Rev.1 Schematic for left, electron upstream, side of HERA e–p interaction region.

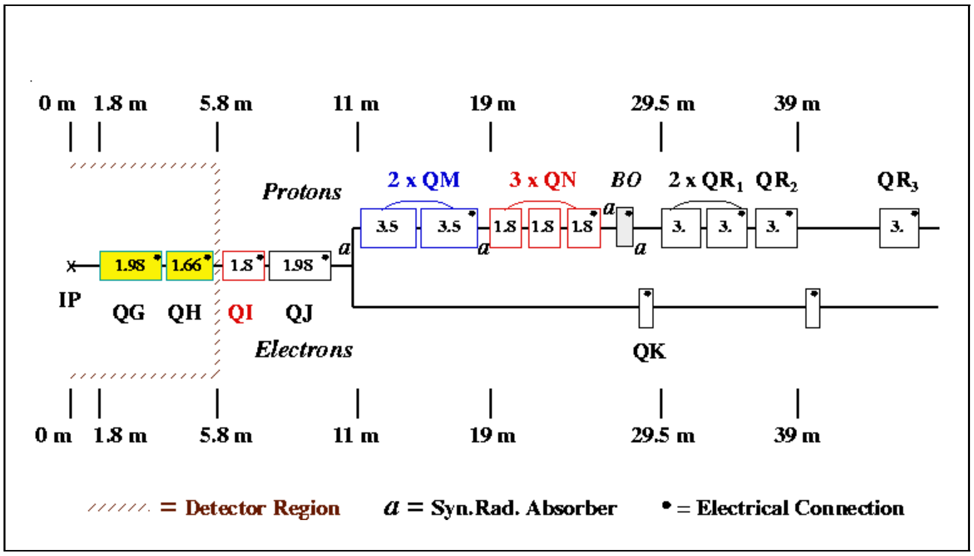

Figure 46: Rev.1 Schematic for right, electron downstream, side of HERA e–p interaction region.

centered on the e–beam so as not to produce excessive synchrotron radiation. A side effect of this positioning of QI and QJ is that the proton beam is quite far off axis in these two magnets and it is the size of this offset as well as the vertical size of the p–beam that determines the minimum aperture for these magnets.

In addition to providing adequate aperture for the p– and e–beams these magnets, QG, QH, QI and QJ, must pass the synchrotron radiation from the upstream magnets. In order to achieve this, special coil geometries, including mid–plane split coils, have to be constructed with associated complex vacuum beam pipes.

The magnetic septum magnets, QM, and current septum magnets, QN, provide the needed vertical focusing for the proton beam while leaving the nearby electron beam unaffected. While most of the synchrotron radiation is still made to pass the QM and QN quadrupoles, it is unavoidable that a high–level of synchrotron radiation would hit the septa without their being

Name	Type	L_m (m)	G_{max} (T/m)	R_p (mm)	B_p (T)	# Req.	Comments
QG	Q + D	1.98	7.6	—	$0.185^\dagger$	4	Air Coil CFM (~104 kW)
QH	Q + D	1.66	6.8	—	$0.260^\dagger$	3	Iron Dominated CFM
QH1	Q + D	1.66	6.8	—	$0.260^\dagger$	1	Air Coil CFM (~166 kW)
QI	Q	1.80	28.	35	0.980	4	Split Coil for Syn. Rad.
QJ	Q	1.98	18.	50	0.900	4	QS/C Profile & Split Coil
QM	Q + D	3.50	25.	37	0.925	8	MSQ with Split Coil
QN	Q	1.80	30.	35	1.050	12	CSQ
BO	D	2.00	—	—	0.950	4	Not Yet Final
QR	Q	3.00	24.	35	0.840	–	Reuse Existing QR Magnets

Table 24: Parameters for Rev.1 Magnets. R_p is the quadrupole pole radius and is omitted where not applicable. †Here instead of B_p we show B_{co} i.e. the value of vertical field at the center of the electron closed orbit.

protected by synchrotron radiation absorption masks.

Beyond these septum quadrupoles are additional dipoles for controlling the proton closed orbit. Also there are additional HERA QR–type quadrupoles, which are moved to new locations closer to the IP, in order to complete the proton interaction region focusing. The main parameters for the Rev.1 magnets are summarized in Table 24.

8.2 Field Quality Requirements

The nominal operating energies of the magnets QI and QJ are $12\,GeV$ (injection) and $29\,GeV$ (luminosity operation). Each magnet should be good enough to allow operation up to $30\,GeV$ and down to $7\,GeV$ without a factor of more than two degradation in field quality. The operating range of the magnets QM and QN corresponds to beam energies of $40\,GeV$ and $820\,GeV$.

The maximum allowed deviation of the magnetic center of the magnet from the geometric center will be denoted by D. D should not exceed 1 mm for the magnets QI,QJ. The magnet QN is less critical. The field center may deviate as much as 5 mm from the geometric center.

The magnet excitation function, $g(I) = [\int Gdl]_I$ is expected to be found within 5×10^{-3} of the predicted value. The design of the magnet should allow to achieve a reproducibility in $g(I)$ of 1×10^{-3}. The gradient in the magnet center should not vary by more than 0.5% for individual magnets in the production process. Saturation and remnant effects are described by a function $S(I)$. Given the definition for $g(I)$ above and its derivative,

$$g'(I) = \frac{d\,[\int Gdl]}{dI}$$

, $S(I)$ is then given by

$$S(I) = 1 - \frac{g(I)}{g(\frac{I_{MAX}}{2}) + g'(\frac{I_{MAX}}{2}) \cdot (I - \frac{I_{MAX}}{2})}.$$

Magnet Name	Reference Radius, R [mm]	$\Delta B/B$ $[1 \times 10^{-4}]$ low excitation	$\Delta B/B$ $[1 \times 10^{-4}]$ high excitation
QI	25	3	3
QJ	25	1	1
QM	25	3	3
QN	25	10	3

Table 25: Field Error Limits for Rev.1 Magnets.

The function $S(I)$ should be smaller than 0.02 everywhere in the nominal operating range of the magnets.

The quadrupole magnets QI, QJ, QN, QM need to be accelerator quality magnets. The field quality must be the same or better than that of other quadrupole magnets in HERA. The sensitivity of the beam to non-linear field errors is enhanced in the insertion regions. This has been taken into account and the corresponding field quality requirements are quite demanding.

The field quality will be defined as the maximum deviation of the field from an ideal quadrupole field at a given reference radius R around the beam axis. This definition includes only nonlinear field errors.

$$\frac{\Delta B(R)}{B} \equiv Max \left| \frac{B(R,\Phi) - G(R=0) \cdot R)}{G(R=0) \cdot R} \right| ,$$

where G is the field gradient

$$G = \frac{d}{dy} B_y = \frac{d}{dx} B_x$$

and $B(R,\Phi)$ is the radial field a radius R and azimuth Φ.

8.3 Air Coil Combined Function Magnet, QG

The quadrupole QG is an unconventional air–coil combined function magnet which provides both vertical focusing and horizontal bending. In concert with the next combined function magnet QH (or QH1) it provides the necessary horizontal bending to separate the electrons from the protons and it also provides an important contribution to the electron focusing so as to help reduce the vertical β–peaks in downstream electron quadrupoles. The focusing provided by the QG and QH magnets is needed to ensure a manageable chromatic contribution to the electron ring dynamics.

Since the QG quadrupoles are placed inside the ZEUS and H1 detectors and are the accelerator magnets closest to the interaction points, magnetic materials such as iron cannot be used in QG due to the presence of ZEUS and H1 detector solenoidal fields. The field configuration inside QG is a combination of quadrupole and dipole field distributions and is achieved via current flowing in copper conductors. The 48 QG conductors are arranged top–bottom symmetric with respect to the median plane as shown in Fig. 47. There is a beam outside gap in the conductor distribution which is needed to pass synchrotron radiation via a horizontally

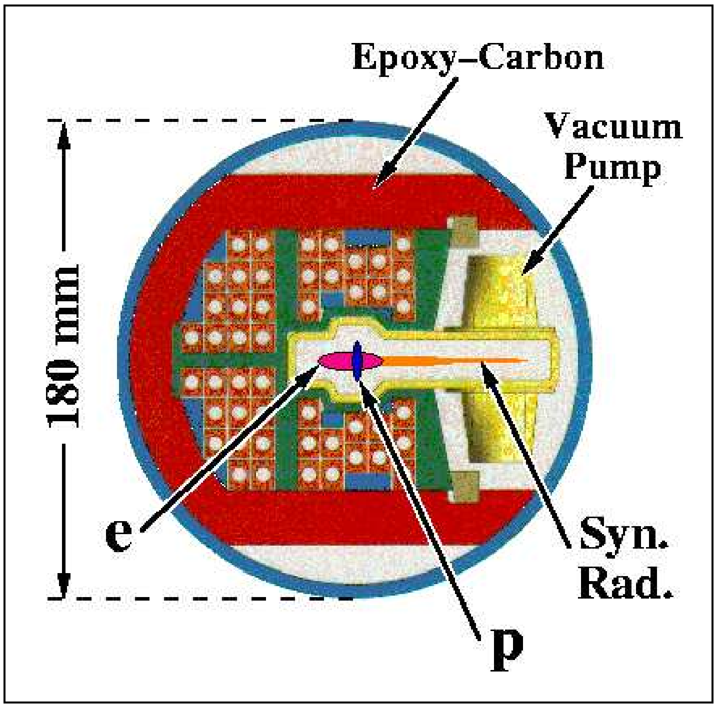

Figure 47: QG Magnet Schematic. Electron, proton and synchrotron radiation beam positions are shown.

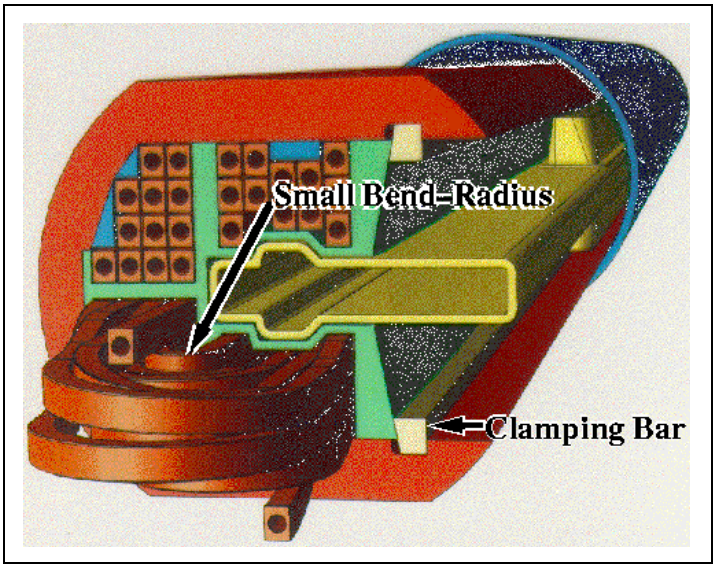

Figure 48: View of QG End showing clamping bar. Note the indicated small–radius conductor bend.

extended vacuum beam pipe. Distributed pumping is provided as indicated in Fig. 47 and Fig. 48 by which the beam pipe and vacuum system are integrated into the magnet.

Four QG magnets are needed each having a design magnetic length of 1.98 m, maximum gradient G =7.6 T/m, and an average vertical field at the electron closed orbit axis of $B_{co} = 0.185$ t. A special design constraint is that this magnet cannot extend transversely beyond a 180 mm diameter circle in order that it can be installed into the central region of the liquid argon calorimeter.

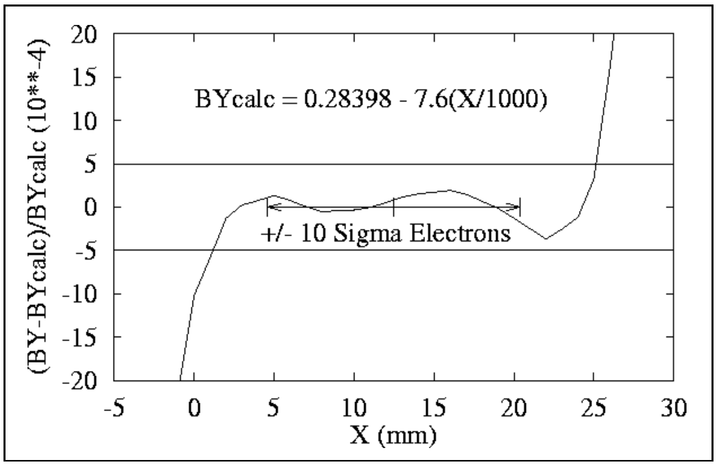

Figure 49: QG Field Quality.

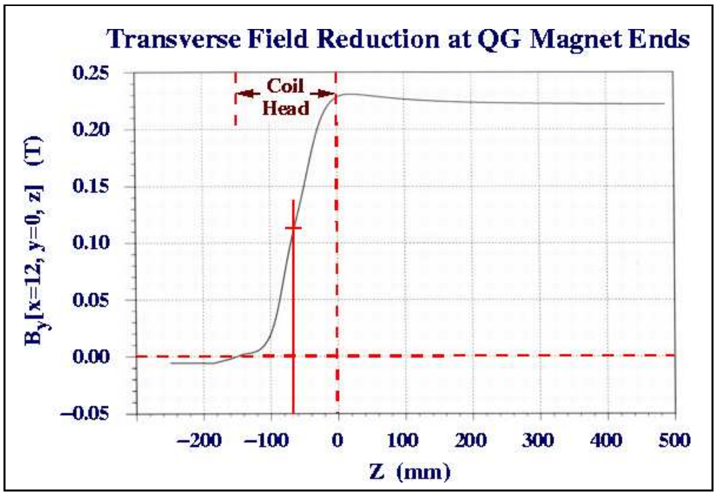

Figure 50: Field Fall Off Near QG End.

The conductor configuration shown in Fig. 47 and Fig. 48 is designed to yield the proper combination of dipole and quadrupole fields with departures from strict linearity over a $\pm 15\,\sigma$ of the electron beam which are less than $\pm 5\times 10^{-4}$ as indicated in Fig. 49. Having no iron or other magnetic material, saturation is not an issue for this magnet and the resulting field is proportional to applied current over its entire operating range. Near the QG ends the transverse field varies smoothly as shown in Fig. 50.

In order to maintain the design field quality of $\pm 5\times 10^{-4}$ it is estimated that the conductor centers should be within ± 0.5 mm of their design positions. To achieve this placement goal special attention has been given to the design of the magnet internal support structure. As shown in Fig. 47 and Fig. 48 the dimensions of the top and bottom coils are assured via the inclusion of an epoxy–glass internal support structure. The combined top and bottom coils and vacuum beam pipe can then be captured in a rigid extruded C–shaped epoxy–carbon structure and are then held in place via a clamping bar assembly. The epoxy–carbon composite material is special in that it has a density lower than aluminum and yet is significantly stronger and more rigid against deformation. As a final step the epoxy–carbon C–structure is attached to an outer cylindrical steel shell for increased mechanical support and rigidity.

The copper conductor cross section is 8×10.7 mm rectangular shape with a 5.8 mm cooling channel and is surrounded on all sides by 0.5 mm insulation. As much as possible, consistent with the desired field quality, conductors are aligned along their edges, without additional spacers, in order to simplify the mechanical configuration. Never the less a significant design challenge exists, as indicated on Fig. 48, in that the innermost conductors are required to make very tight bends. The tightest bend radius is about equal to the conductor width and would have an unacceptably large "keystoning" if made with conventional bending techniques. It is possible to make such tight bends with short sections of conductor filled with "sand." So the present QG construction scenario has these tight bends being made separately and then being joined (brazed with short adaptor pieces) to the straight sections. The outer larger radius bends can then be formed around the inner layers. Other techniques are being investigated for forming the tight inner bends; however, it seems unavoidable to have to braze the inner conductors to their respective straight sections.

Another important issue for the QG magnet is that of power dissipation and water cooling. In order to reach the design gradient of 7.6 T/m the QG magnet must be energized with close to 2000 Amps. With the conductor cross section and magnet dimensions given above this maximum current translates to a power dissipation of 104 kW. By taking care in the design to provide sufficient parallel cooling circuits to limit the peak water flow rate in the magnet to about 2 m/s and by cooling the magnet with reduced temperature (i.e. chilled) water, the magnet temperature can be kept low enough so as not to disturb detector components.

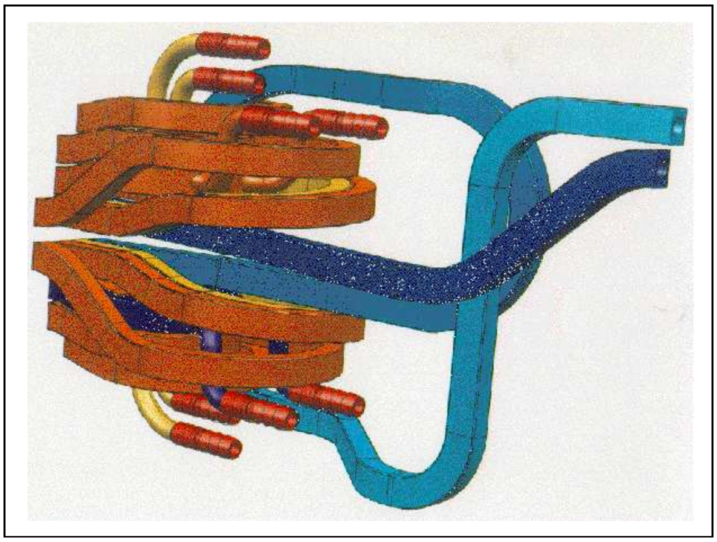

Figure 51: Conceptual Scheme for QG Current Lead and Water Connections.

It is intended to keep the QG end closest to the interaction point simple and only have the current and water flow turn around at this end. The side away for the interaction point is the preferred point for necessary water manifold connections, lead connections and top–to–bottom coil connections as indicated with Fig. 51.

8.4 Combined Function Magnet, QH

The QH combined function magnet, shown in Fig. 52, while functionally very similar to the previous magnet QG, differs in one very important respect; unlike QG, the QH magnet uses magnetic material to capture and shape the field generated from its excitation coils. The

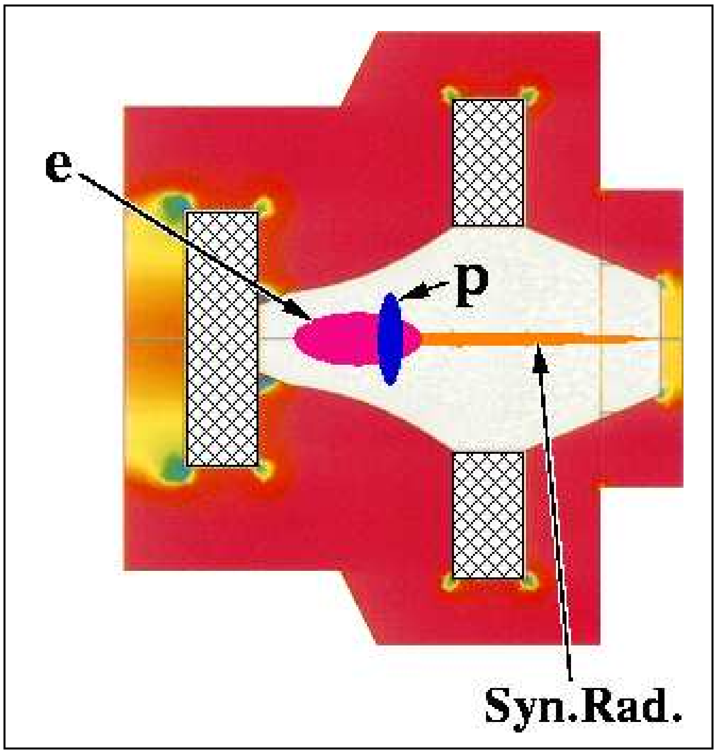

Figure 52: QH Magnet Schematic. Electron, proton and synchrotron radiation beam positions are shown.

intrinsic power consumption of the QH magnet is only a small fraction of that of the QG magnet in spite of the QH's larger aperture. Also an important benefit for the ZEUS experiment is that because the iron confines the region of high field to inside the magnet, the stray leakage field seen by FCAL phototubes located close (≈120 mm) to the beam axis is substantially reduced compared to the use of an ironless combined function magnet.

One drawback for the use of magnetic material in QH is that it may only be placed in regions outside the detector solenoids. For the ZEUS experiment this is not an important consideration as QH can be used in both the electron upstream (experiment forward) and downstream (experiment backward) sides; however, for H1 the electron upstream side is inside the detector solenoid so QH can only be used on the electron downstream side. For the H1 electron upstream side an ironless combined function magnet, similar to QG, must be used. This magnet, QH1, is described in the next subsection.

The iron dominated combined function magnet, QH, has a design magnetic length of 1.66 m, maximum gradient $G = 6.8$ T/m and an average vertical field at the center of the closed orbit, $B_{co} = 0.260$ T. Three such magnets are required (2 for ZEUS and 1 for H1).

By intent B_{co} is smaller in the QH separator magnet than in QG in order that the QH synchrotron radiation, which hits the innermost absorbers closest to the interaction point, has a lower critical energy than that from QH. By this means the backscattering from the synchrotron radiation absorbers closest to radiation sensitive central detector elements is reduced.

The somewhat exotic iron cross section for the QH magnet is the result of satisfying the following diverse design goals:

- Reach as high as feasible quadrupole gradient.

- Provide large–horizontal good field region for electrons.
- Keep stray field low in upstream ZEUS FCAL.
- Pass all synchrotron radiation through downstream aperture.
- Fit inside the ZEUS FCAL
- Provide right–of–ways for survey and alignment monitoring, and for passing power and cooling to QG

One means to satisfy the first three goals is to have a closed geometry with an outside plate to capture the magnet flux which would otherwise be present outside the gap of an open combined function magnet geometry. In order to achieve the 6.8 T/m quadrupole gradient the magnetic pole must have a significant curvature and it is found useful to utilize a taper section, extending from the coil edge to the plate, for field shaping purposes.

To satisfy the next two goals, passing the downstream synchrotron radiation and fitting inside the ZEUS FCAL, requires further optimization of the plate geometry. Of course the position of the inner edge of the plate is constrained by synchrotron radiation geometry to be sufficiently far out. Fortunately, because of the relatively low nominal field, B_{co} of 0.26 T and the combined function geometry (quadrupole and dipole field contributions opposite sign on beam outside side) it is possible to contain the flux with a thin plate.

Taking into account the thinness of the flux plate, the inward beam offset for the electrons and the synchrotron radiation geometry, it is possible to approximately center the QH magnet in the space available in the ZEUS FCAL. Also because of the relatively low fields involved and associated small saturation of large regions of the iron, it is possible to make deep cuts, as shown on Fig. 52, in order to satisfy the last goal of providing right–of–ways, without unduly spoiling the magnetization distribution in the iron.

8.5 Combined Function Magnet, QH1

The QH1 combined function magnet is similar to QG in that it too is an air–coil magnet; however, the QH1 parameters must be matched to those of QH. It has a design magnetic length of 1.66 m, maximum gradient $G = 6.8$ T/m and an average vertical field at the center of the closed orbit, $B_{co} = 0.260$ T. Only 1 such magnet is required for the electron upstream side of H1.

Even though the gradient and length of QH1 are both less that those of QG one might expect that its power consumption could be smaller than that of QG; however, QH1 requires a significantly larger good field region than QG and with the constraint that both magnets have to fit within the same transverse space requirements of the H1 cryostat, 180 mm diameter, the space available for copper conductors is reduced inside of QH1. The result is that the power consumption of QH1 at maximum gradient is estimated to be 166 kW. In point of fact there would be no satisfactory conductor configuration for QH1 that maintains the current density in the copper below a manageable level of 20 A/mm^2 if it had to satisfy the same synchrotron radiation aperture requirements as the downstream side QH.

Since QH1 is only used on the upstream side of the interaction point the only appreciable synchrotron radiation which has to pass through it is what is generated by QI, QJ and itself.

Over QH1's 1.66 m length the synchrotron radiation has barely separated from the 20σ contour of the electron beam and it is possible to find extra space to place conductor windings very close to the horizontal axis outside the beam. The 166 kW estimate for power consumption is based upon such a design configuration.

The design requirements for QH1 are similar to those of QG, and many of the design considerations discussed in the earlier subsection on QG apply here; however, there are two additional design considerations:

- Using all available space for conductor windings means that there is no room for distributed vacuum pumping inside the QH1 magnet.
- The ≈2000 Amp current leads to the QG magnet have to pass unshielded through QH1.

Not having pumping over the 1.66 m has to be budgeted for in setting the pumping speed capacity in this region. As for the QG current leads the issue is minimizing the stray field seen at the beam position. One can minimize this by pairing the QG current leads and passing them through the space at the top or bottom of the QH1 magnet. Provision for this is allowed for in the QG design.

8.6 Horizontally Focusing Quadrupole, QI

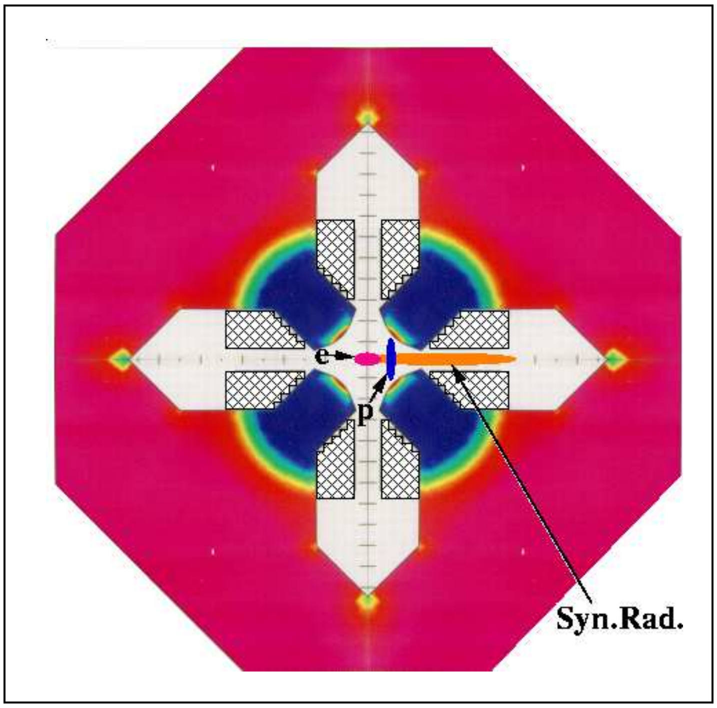

Figure 53: QI Magnet Schematic. Electron, proton and synchrotron radiation beam positions are shown.

The quadrupole QI is an almost conventional quadrupole magnet. Its special feature is that this magnet has to provide room for the synchrotron radiation fan in the magnet mid-plane as shown in Fig. 53. The space between the return yoke and the beam chamber is thus kept free for the synchrotron radiation to pass through.

The QI magnet has a length of 1.8 m, a maximum gradient of 28 T/m, and a pole radius of 35 mm. A total of four magnets will be needed.

8.7 Vertically Focusing Quadrupole, QJ

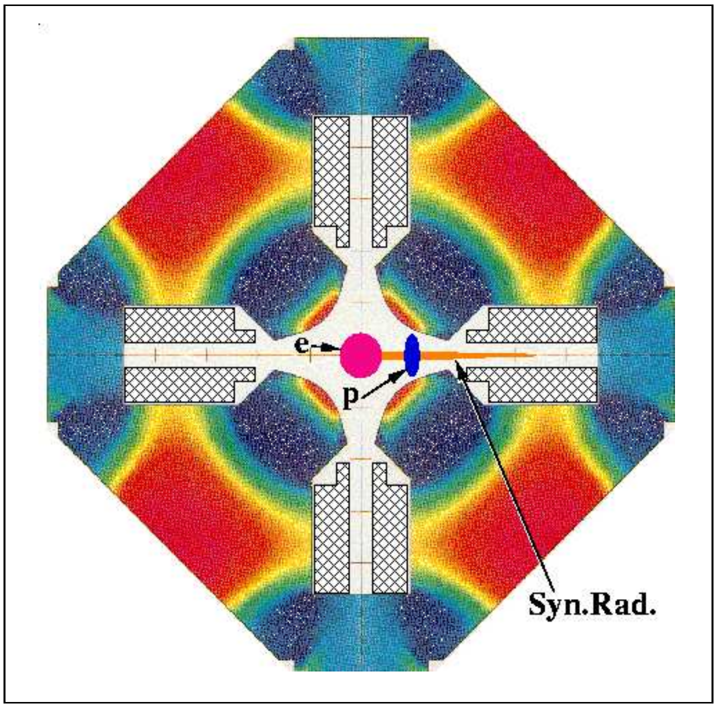

Figure 54: QJ Magnet Schematic. Electron, proton and synchrotron radiation beam positions are shown.

Like the previous magnet QI, the quadrupole QJ also needs to maintain free space for the synchrotron radiation as shown in Fig. 54. It has a larger radius of 50 mm and a length of 1.98m. Its maximum required gradient is 18 T/m. A total of four magnets will be needed. The choice of 50 mm for the aperture of this magnet permits the use of existing HERA QC/QS lamination profiles as shown in Fig. 54 with only a modified split coil cross section to accommodate the synchrotron radiation fan.

8.8 Magnetic Septum Quadrupole, QM

The magnet QM is a septum half–quadrupole and is used to focus the proton beam. This magnet has a mirror plate with a deep cut out to provide a field free region for the electron beam as shown in Fig. 55. The magnet mid-plane opposite the mirror plate is also kept free for the synchrotron radiation fan.

The magnet has a length of 3.5 m. Two such magnets will be placed together and powered in series. The maximum gradient of the magnet is 25 T/m. The pole radius is 37 mm. A total of 8 magnets will be needed.

Additional correction coils located in the septum cut–out and inside the magnet aperture ensure the necessary field quality.

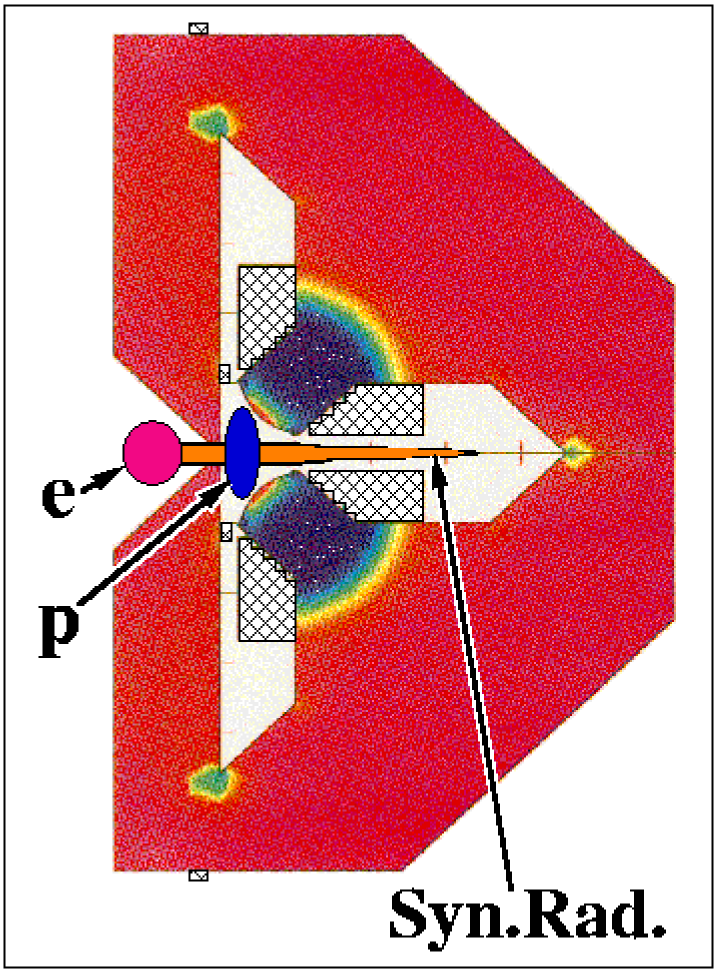

Figure 55: QM Magnet Schematic. Electron, proton and synchrotron radiation beam positions are shown.

8.9 Current Septum Quadrupole, QN

The magnet QN is a septum quadrupole with a narrow septum coil as shown in Fig. 56. The septum coil has large current density as the full N×I amp·windings of the main coils have to pass through the septum area. The magnet mid-plane opposite the septum coil is once again kept free to pass the synchrotron radiation fan.

This magnet has a length of 1.8 m and 3 such magnets will be placed together and powered in series. The maximum gradient of the magnet is 30 T/m. The pole radius is 35mm. A total of 12 magnets will be needed.

8.10 Horizontally Focusing Quadrupole, QR

Taken together the QM and QN quadrupoles work optically as the first vertically focusing lens of an optical doublet for the proton beam. Existing QR quadrupoles are shifted from their present locations and moved closer to the interaction point in order to make up the final horizontally focusing lens of the doublet.

At their new locations some of the QR magnets require modification in order to accommodate the electron vacuum beam pipe. This modification consists of grinding away some of the

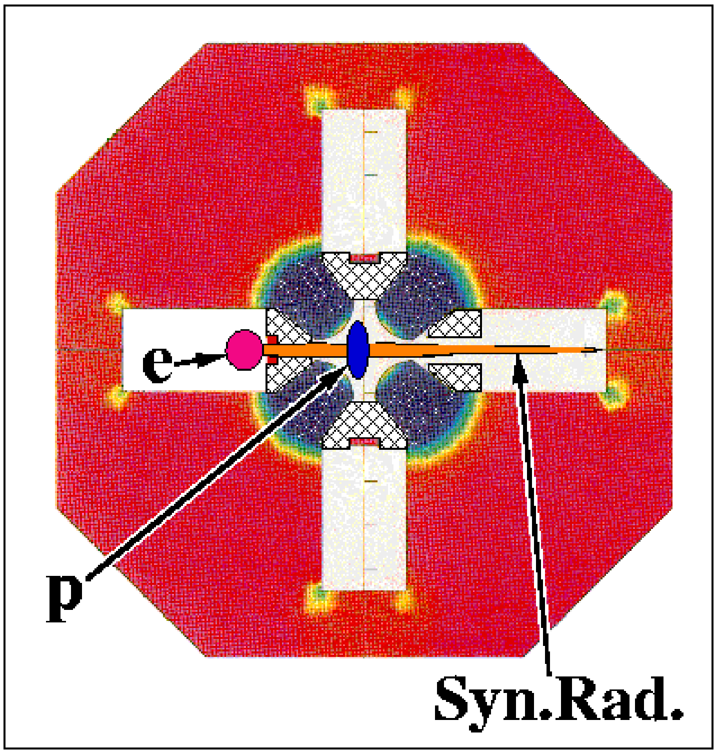

Figure 56: QN Magnet Schematic. Electron, proton and synchrotron radiation beam positions are shown.

magnet yoke and clamping bolts in order to place the electron beam pipe as close as possible to the proton beam line and adding additional inboard clamps, through which the electron beam pipe can pass, to hold the affected QR magnets together. It is anticipated that 8 QR magnets must be so modified.

8.11 Superconducting Separator Magnets, QO, QG, and QH and Changes Possible with a Rev.2 Lattice

During the course of the Luminosity Increase Subgroup Studies it was realized that chromatic effects associated with the smaller electron horizontal– and especially vertical–$\beta^\star$, with the correspondingly higher β–peaks and stronger focusing, could well prove to be the limiting factor in increasing HERA luminosity and this has been born out in tracking studies. One way to reduce the interaction region chromaticity is to introduce some focusing closer to the interaction point, i.e. inside the ZEUS and H1 detectors. This has been done, to some extent, by turning the separator dipoles into the combined function magnets, QG and QH (QH1). Unfortunately the limit to what is practical to achieve in terms of current density and water flow in a copper conductor falls ever so slightly short of achieving a high enough quadrupole gradient. Also the small inner aperture needed to achieve this gradient and dense packing of copper conductors around the beam lead to modification of the energy deposition in calorimeter areas close to these magnets and can thereby affect low Q^2 detector response.

We have therefore investigated alternate technologies and find that superconducting magnets could provide a better match to the HERA Upgrade needs. Superconducting coils:

- Can easily be nested with dipole and quadrupole windings for a tailored combined function magnet.
- Can be made with large apertures to pass synchrotron radiation and other forward– or backward–going reaction particles.
- Can have higher gradients in spite of having a large aperture due to the more than an order of magnitude higher achievable current density.
- Dissipate less energy inside the experiments.
- Naturally lead one to consider cryopumping solutions for the vacuum region near the experiment.

Of course there is significant engineering complexity in designing a small cryostat to fit inside the experimental detectors; however, at present we have found no "show stoppers." If one then takes a superconducting solution as the basis for a new Rev.2 lattice, one is led to ask how such a Rev.2 lattice will differ from the Rev.1 version discussed so far.

While at the time of this writing a compete Rev.2 lattice does not exist in all details, some general features have emerged:

- Proton magnets QM, QN and QR remain.
- Both experiments can use the same magnet solution (i.e no special QH1 just for H1).
- Preferred solution has a single superconducting magnet $\approx$3.4 m long, denoted QO (Q "oh") on left against two shorter and larger aperture magnets, $\approx$2.0 and $\approx$1.6 m long, still denoted QG and QH on the right.
- QO, QG and QH gradients are in the range 10–13 T/m and help to reduce electron peak–βs from 350 m to around 180 m.
- QO, QG and QH each have independent dipole windings for better closed orbit control than possible with the resistive option.
- The optimal lengths for QI and QJ change only slightly (lengths becoming equal, 1.88 m) due to additional vertical focusing.

In addition to the above, the most natural configuration for the separation geometry moves the effective bend center closer to the interaction point. The result of this shift is to increase by a few mm the separation of the proton and electron beams in the QI quadrupole. It would seem prudent to increase the QI aperture from 35 to 37 mm to insure adequate proton aperture in this magnet.

At the point that a superconducting combined function separator magnet design, Rev.2 lattice, becomes available it is expected that it will become the preferred design. The resistive separator magnets and associated Rev.1 lattice describe above will then become the backup option.

References

[1] "PEP-II Conceptual Design Report," Chapter 5, Lawrence Berkeley Lab. PUB-5379, 1993.

[2] M. Marx, B. Parker and H. Wümpelmann, Concept for a New Magnet Septum Quadrupole, European Particle Accelerator Conference, Barcelona, Spain, June 1996. See DESY Internal Report DESY M 96–13, July 1996 or http://www.desy.de/~parker/EPAC96/mop040g.ps on World Wide Web.

8.12 Design of the QG Magnet

Two types of designs were considered for the air core magnet (QG): a design using Al collars as coil support and a second design with a DUROSTONE inner support, which is the prefered solution. Detailed calculations of the collar deformation were performed for the Al collar design. The deformations of the DUROSTONE based design will be even smaller than for the Al collar, because of the higher bending and tensile moments of elasticity.

8.12.1 Technical Layout of the QG Magnet

The air coil combined function magnet QG is located close to the IP (1.8 m to 3.8 m) inside the experiments H1 and ZEUS. The welding seams inside the H1 liquid argon tank define the 180 mm outer diameter of the magnet support-pipe which contains the magnet collar fixing the coil in a coil trough.

Magnet parameters The main magnet parameters are give in table 26.

Magnet Parameters	
windings per coil	12
field gradient	G = 7.6 T/m
magnet length	Lm = 1,98 m
winding length per coil	= 45.73 m
coil resistance	R = 13.36 mΩ
magnet resistance	Rm = 26.72 mΩ
rated current	I = 1955 A
voltage drop	U = 52 V
power consumption per coil	Psp = 51 kW
power consumption per magnet	Pm = 102 kW
temperature difference	ΔT = 40 K
waterflow per coil	V = 0.31 l/s
cooling circuits per coil	6
water speed per cooling circuit	v = 1.92 m/s
pressure drop per cooling circuit	Δp = 0.82 bar

Table 26: Parameters of the QG magnet.

Coil Manufacturing The coil will be made using a hollow Se-Cu conductor of 10.7x8 mm size with a 5.8 mm inner bore for cooling. The coil heads of the first layers and the water connection pieces are made by investment casting, forgging or selective laser sintering and brazed to the long straight conductors. The outer layers are wound conventional. Fig. 57 shows the coil head with the connections for cooling pipes.

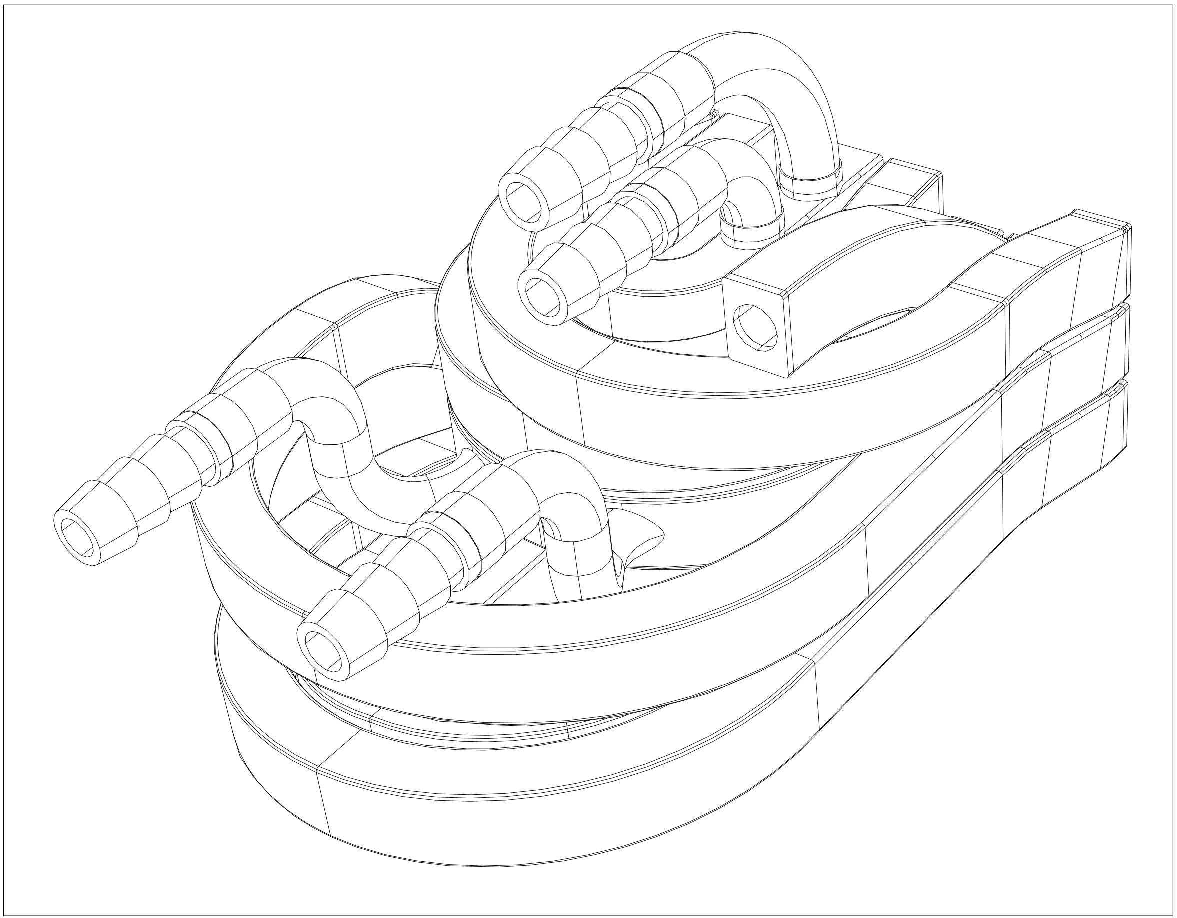

Figure 57: Coil head of QG magnet including connections for cooling pipes.

After all brazings are made, the layers are split vertical and wrapped with glass tape 0.13 mm half overlapped. Then the layers are compressed again, the spacers are put in place and the outer insulation is made. To get a stiff, rigid and accurate to size coil body, the coil is vacuum impregnated.

Magnet assembly The two coils are put into a H-shaped "coil trough" (see Fig. 58) made from DUROSTONE VEGM-LP. To close the trough, there has to be bonded one layer of KAPTON on top and bottom of the coil. The complete coil is shifted into the magnet collar made from DUROSTONE VEGM-CA as shown in Fig. 59 and fixed by clamping one of the H-bars of the trough by bolting the taper gib to the collar. In addition the other H-bar of the trough is fixed by M6 bolts to the collar. After connecting the coils the whole magnet is shifted into the magnet support pipe as display in Fig. 60 and Fig. 61.

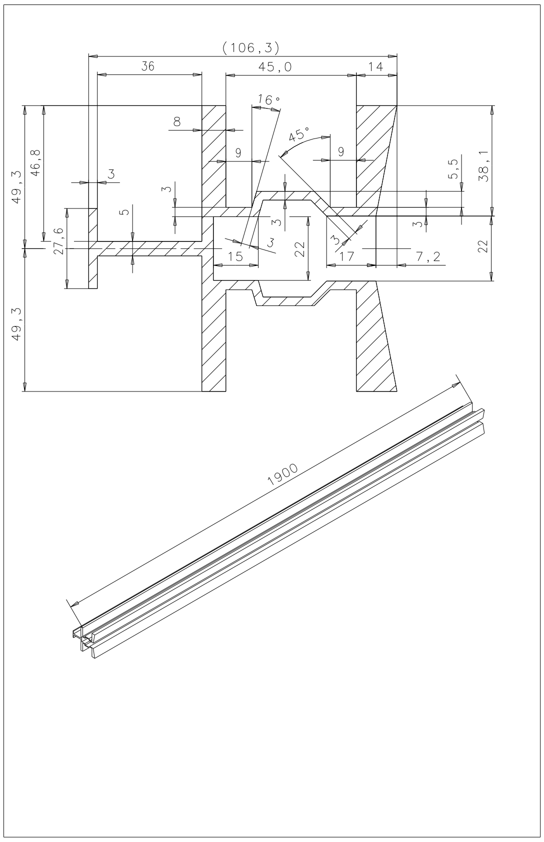

Figure 58: Inner support of QG magnet.

Materials A comparison of possible magnet collar and coil trough materials is shown in table 27. The (in most cases) better properties of DUROSTONE recommend this material for magnet collar and coil trough. Even the magnet support pipe could be made from DUROSTONE VEGM-CA.

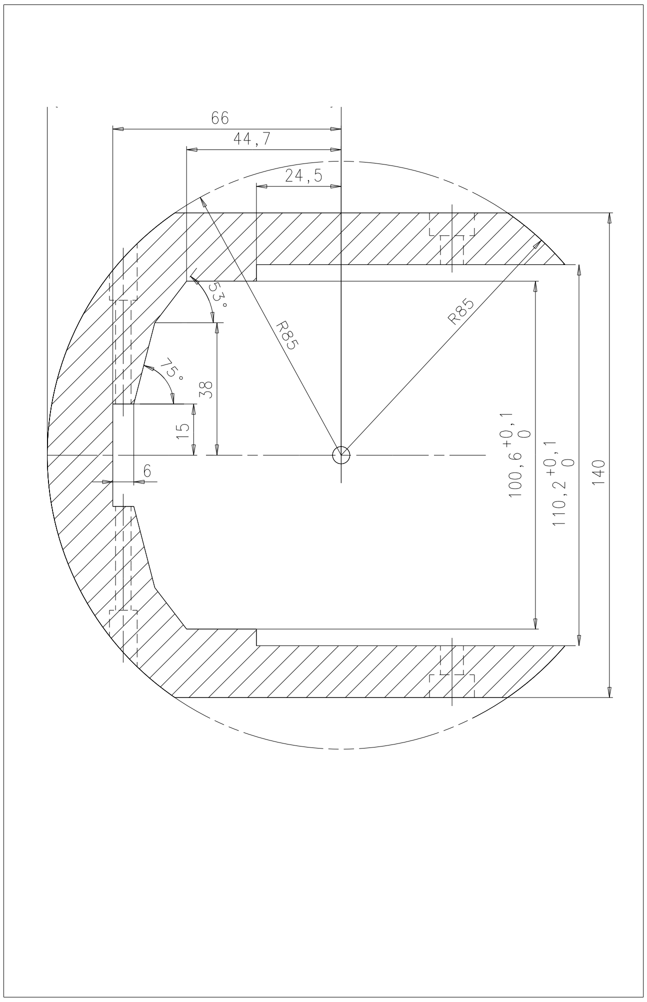

Figure 59: Durostone VEGM-CA collar of QG magnet.

Material Properties				
material	Durostone	Durostone	Aluminium	Stainless Steel
	VEGM-CA	VEGM-LP	AlMg7	1.4301
carbon content (%)	50	-	-	
glass fiber content (%)	-	60	-	
density (g/cm^3)	1.50 - 1.65	1.75 - 2.10	2.7	7.9
radiation length (cm)	23.75	18.50	8.90	1.76
heat conductivity (W/m/K)	≈0.30	≈0.30	204.0	15.0
bending moment of elasticity (N/mm^2)	70-90$\cdot10^3$	15-30$\cdot10^3$	69$\cdot10^3$	200$\cdot10^3$
bending strength (N/mm^2)	450-500$\star$	350-400$\star$	120	490
tensile module of elasticity (N/mm^2)	165$\cdot10^3$	20-25$\cdot10^3$	69$\cdot10^3$	200$\cdot10^3$
tensile strength (N/mm^2)	700†	350†	340	600

Table 27: Comparison of properties of possible materials used as magnet collars and trough for the combined function magnet QG. $\star$ indicates bending strength perpendicular to laminated surface. † indicates tensile strength parallel to laminated surface.

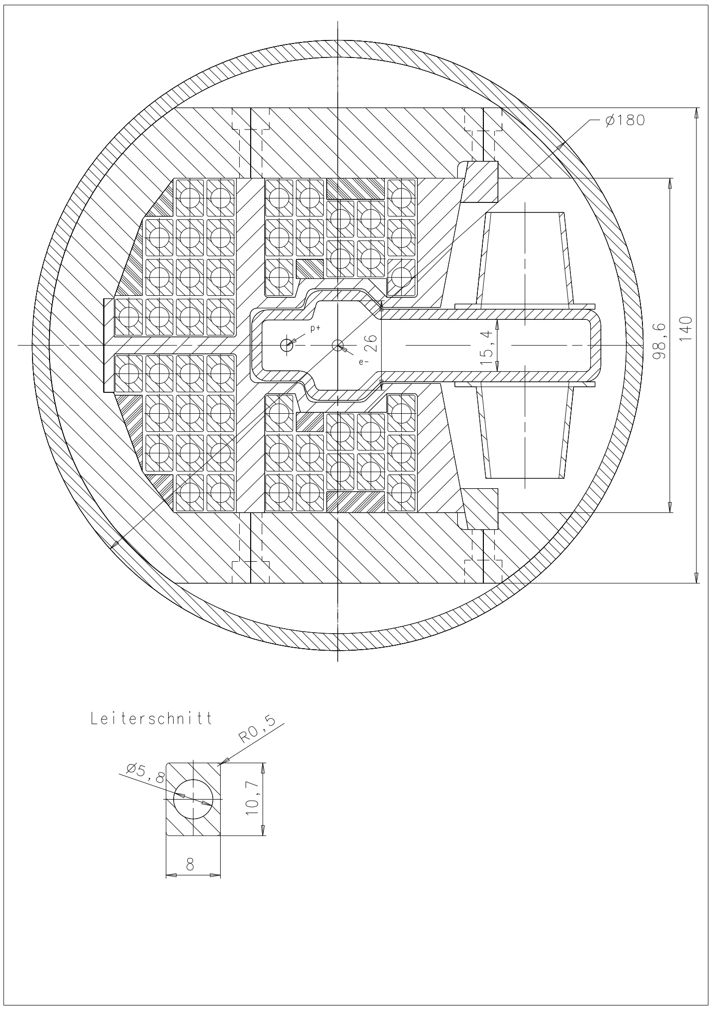

Figure 60: Cross section of QG magnet including outer support tube.

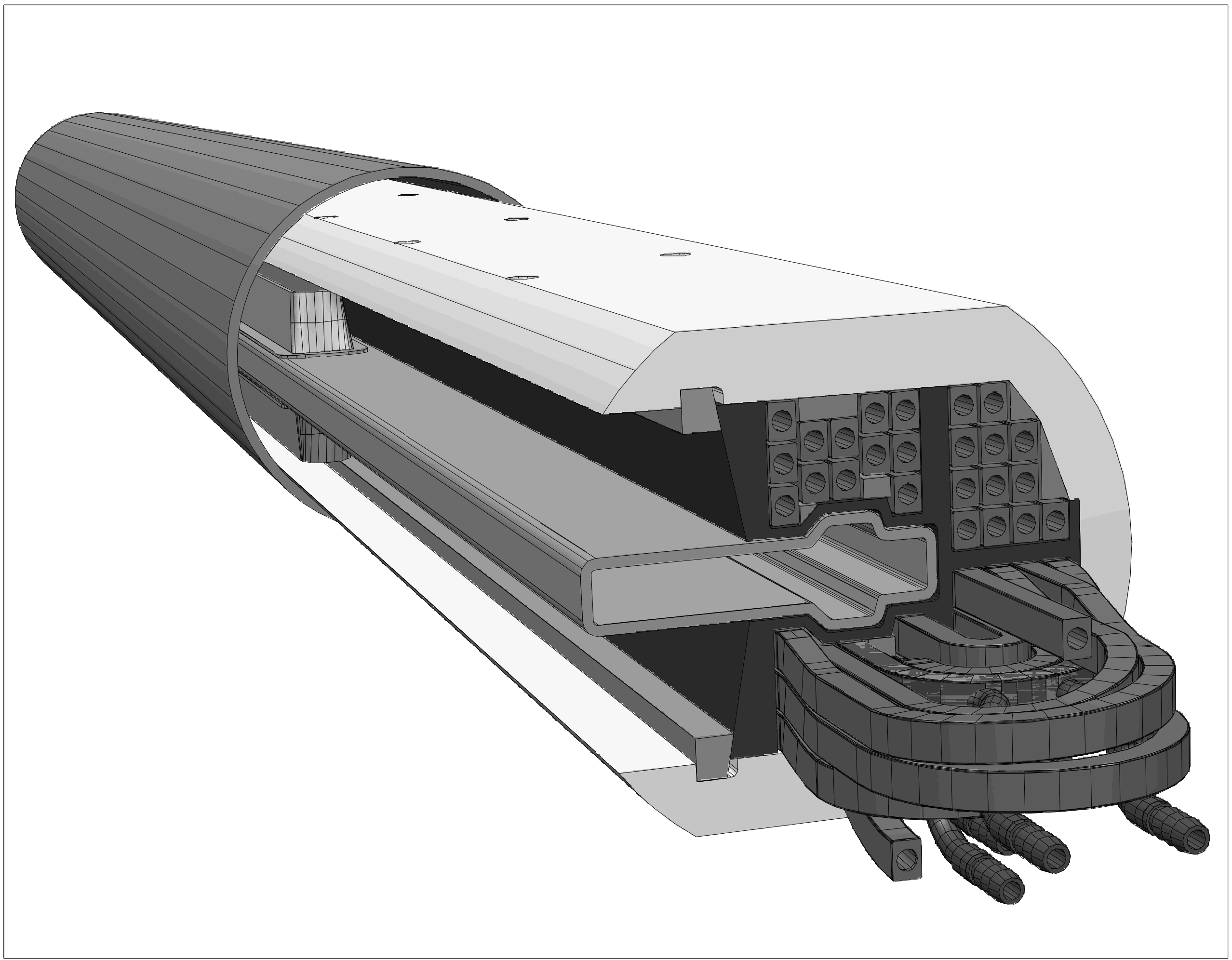

Figure 61: Three dimensional display of QG magnet.

8.12.2 Design of Collared Combined Function Magnet

Description The idea of a collared magnet is based on a design of two coil halves, an upper and a lower half, which will be assembled using pre-stacked collar sheets. Both halves will be closed and locked together.

The collars will be made out 4 mm thick punched aluminium sheets. Because of the coil symmetry in only one plane, two collar types are necessary. Alternating types will be stacked together and supported by steering rods. Each collar pakets will be fixed and pressed together by threats at either end of the steering rods. A kapton foil (about 0.1 mm thick) will be placed between the collar paket and the coil for electrical insulation and in order to reduce the friction between collars and coils.

After installation of the coils into the collar pakets, both halves will be assembled, pressed together in a fixture and fixed by rods with threads. Fig. 62 shows a cross section of the complete magnet mounted inside the ZEUS detector.

Calculation of collar dimensions The following boundary conditions were taken into account for the collar dimensions:

- The forces between individual coil conductors of $F_x = 2.9\,kN/m$.
- The outer dimension of the collars was fixed by the available space inside the H1 and ZEUS detectors.
- The collars are made out of 4 mm thick AlMg3 sheets.

The collar nose The collar nose is the collar part above and below the beam pipe, on the open side of the 'C' shaped magnet. The load on the unsupported end of the collar nose is given by

$$F_c = 2.9 \cdot 10^3 \frac{4}{1000}\,N = 11.6\,N.$$

The bending moment at the transition to the rest of the collar is:

$$M_{b1} = F_c \times l = 371.2\,mmN\,,$$

where $l = 32\,mm$ is the jib length of the collar nose. Using

$$W = \frac{b_1^2 \times d}{6} = 66.67\,mm^3,$$

the stress at this transition is

$$\sigma = \frac{M_{b1}}{W} = 5.57\,N/mm^2,$$

which is much lower than the allowed stress of $\sigma_{allowed} = 53\,N/mm^2$. The deflection of the free end of the collar nose is given by the following differential equation

$$w''(x) = \frac{M(x)}{E \times J(x)}.$$

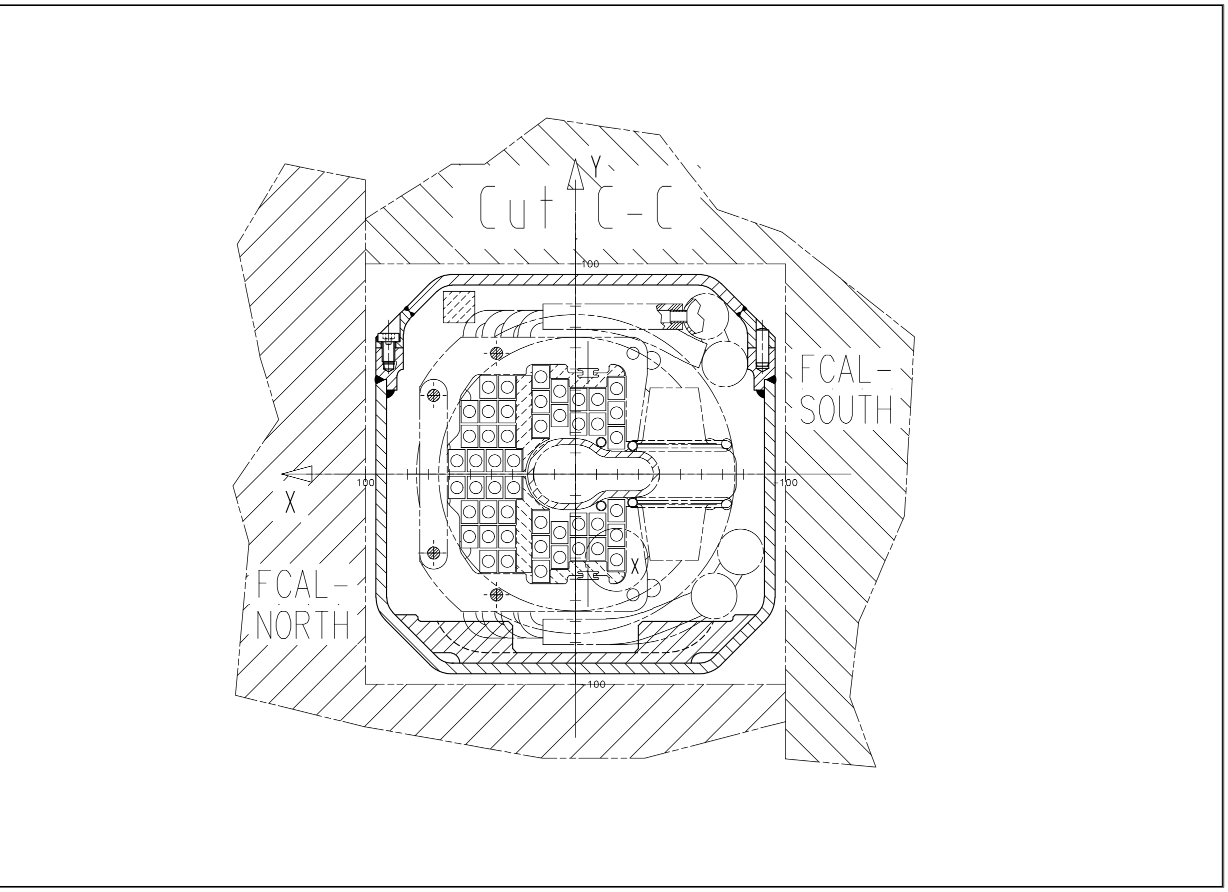

Figure 62: Cross section of the Al collar QG magnet mounted inside the ZEUS detector.

Integrating twice and taking into account the boundary conditions, the deflection is:

$$w(x=0) = \frac{12F_c}{Ed}\times[-\frac{1}{\delta^3}\ln\delta^2 b_0 - \frac{1}{2\delta^3} + \frac{1}{\delta^3}\ln(\delta^2 b_0 + \delta^3 l) + \frac{b_0}{2\delta^3(b_0+\delta l)} - \frac{l}{\delta^2(b_0+\delta l)} + \frac{b_0 l}{2\delta^2(b_0+\delta l)^2}]$$

Assuming a Young's modulus of $E = 7\times 10^4\ N/mm^2$, $d = 4\,mm$, $b_0 = 5.6\,mm$, $b_1 = 10.0\,mm$, $l = 32\,mm$ and $\delta = \frac{b_1 - b_0}{l} = 0.1375$, the result is:

$$w(x=0) = 8.23\cdot 10^{-3}\,mm.$$

The main collar The main collar, except the nose part, is calculated assuming a continuous girder supported on four bearings. These bearings correspond to the two rods used for locking of both magnet halves (bearings A and B), and the steering rods of the collar paket (bearings C and D). The collar can be devided into 3 pieces (bars):

$$A \longleftarrow < bar1 > \longrightarrow B \longleftarrow < bar2 > \longrightarrow C \longleftarrow < bar3 > \longrightarrow D$$

The length of the three pieces are $l_1 = 75\,mm$, $l_2 = 36\,mm$ and $l_3 = 51\,mm$. Bars 1 and 3 have a height of 13 mm, bar 2 a height of 18 mm. The moments of inertia are: $J = \frac{d \times h^3}{12}$; $J_1 = J_3 = 732\,mm^4$ and $J_2 = 1944\,mm^4$.

The load on the complete girder system is given by the clamping moment at the collar nose $M_{b1} = 371.2\,mmN$ and the force due to the first and fourth coil paket of $R = 23.2\,N$. The origin of this force is at $\frac{l_1}{2}$.

Balancing of moments according to Cross results in bearing moments of $M_A = 0\,mmN$, $M_B = -279.5\,mmN$, $M_C = +173.5\,mmN$ and $M_D = -371.2\,mmN$ for the complete girder system. The maximum moments on the girder occur at $\frac{l_1}{2}$ and are

$$M_{l_1/2} = \frac{1}{4} R l_1 + \frac{1}{2} M_B = +295.5\,mmN.$$

All the moments cause stresses inside the collar, which are much smaller than the maximum allowed stress of $\sigma_{allowed} = 53\,N/mm^2$. The resulting forces on the bearings are:

$$A = \frac{1}{2} R + \frac{M_B - M_A}{l_1} = 7.87\,N,$$

$$B = \frac{1}{2} R + \frac{M_A - M_B}{l_1} + \frac{M_C - M_B}{l_2} = 27.91\,N,$$

$$C = \frac{M_B - M_C}{l_2} + \frac{M_D - M_C}{l_3} = -23.26\,N,$$

$$D = \frac{M_C - M_D}{l_3} = 10.68\,N.$$

These bearing moments cause loads on the collar steering rods, and would result in elastic deformations if the magnet was not firmly attached to the trough. The maximum pressure occurs at position B. Using a rod diameter of 6 mm it is $\sigma_l = \frac{B}{6 \times 4} = 1.16\,N/mm^2$, which is negligible compared to $\sigma_{allowed}$.

Deflection of collar nose and maximum deflection of bar 1 The rotation of the bending line is:

$$w'(x) = \frac{1}{E \times J} \times \int_0^l M(x) dx = \tan\alpha.$$

According to Mohr, the rotation at bearing D is:

$$\tan\alpha = \frac{1}{EJ_3} \times [\frac{1}{3}|M_D| l_3 - \frac{1}{6} M_C l_3] = 9.437 \cdot 10^{-5}.$$

Multiplying by the level arm of 43 mm, and adding the deflection, the total deflection of the collar nose is $f_{max} = 1.23 \cdot 10^{-2}\,mm$.

The maximum deflection of bar 1 (there is a non-continuity at the origin of force R) is obtained by solving the differential equations

$$w''(x) = \frac{1}{EJ}[Ax + \frac{M_B}{l_1}x] \quad \text{for} \quad 0 < x < \frac{l_1}{2}$$

and

$$w''(x) = \frac{1}{EJ}[Ax + \frac{M_B}{l_1}x - R(x - \frac{l_1}{2})] \quad \text{for} \quad \frac{l_1}{2} < x < l_1.$$

Taking into account the boundary conditions $w(x = 0) = 0$ and $w'(x) = 0$ for the position of the largest deflection of, the results are $x_1 = 15.28\,mm$ and $x_2 = 76\,mm$. The position x_2 is outside of the bar length and therefore not significant. x_1 is within the region of $0 < x < \frac{l_1}{2}$ and therefore the position of largest bending of

$$w = \frac{1}{6EJ}x_1(A + \frac{M_B}{l_1}) = 4.81 \cdot 10^{-5}\,mm.$$